A Hybrid 3DMLUV-ACA Method for Scattering from a 3-D PEC Object above a 2-D Gaussian Dielectric Rough Surface

C. Li[1], S. Y. He[1], G. Q. Zhu[1], Z. Zhang[2], F. S. Deng[3], B.X Xiao[4]

[1] School of Electronic Information
Wuhan University, Wuhan, 430079, China
whunpredestiny@gmail.com, siyuanhi@gmail.com, gqzhu@whu.edu.cn

[2] HuaZhong Agricultural University, Wuhan Hubei 430079, China
zhangzhe203@163.com

[3] Wuhan Maritime Communication Research Institute, Wuhan Hubei 430079, China
dengfs2009@gmail.com

[4] Geophysics Engineering Center, Chang Jiang University, Jingzhou Hubei 434023, China
npredestiny@yahoo.com

***Abstract*—** The bistatic electromagnetic scattering from the composite model of a three-dimensional (3-D) arbitrarily shaped object located above a two -dimensional (2-D) Gaussian rough surface is analyzed in this work. The object suited above is assumed to be a perfect electric conductor (PEC) while the rough surface is dielectric. Firstly, the Poggio, Miller, Chang, Harrington, Wu and Tsai (PMCHWT) integral equations, electric field integral equation (EFIE) are implemented and extended on the rough surface and on the surface of the object respectively. Then, the method of moments (MoM) combined with Galerkin method is introduced to discretize the integral equations to the matrix form using RWG basis function. Due to the memory requirement and computational complexity of traditional MOM are $O(N^2)$ (N is the number of unknowns), the rank based 3-D Multilevel UV method (3DMLUV) is employed to reduce memory and CPU time overhead. The 3DMLUV has been successfully applied in the scattering of PEC targets, however, when the object or rough surface become dielectric, the fast fill-in method proposed in Reference [19] often breaks down due to the oscillatory nature of the gradient of Green's function. Therefore, the ACA is applied to speed up the filling of the impedance entries required in 3DMLUV because of its algebraic nature. The efficiency and accuracy of the proposed method are demonstrated in a variety of scattering problems.

Index Terms - Composite model, bistatic scattering, PMCHWT, 3DMLUV, ACA

I. INTRODUCTION

Electromagnetic (EM) scattering from an object above a rough surface has attracted much interest during recent years, because of its extensive applications to remote sensing, target recognition, radar surveillance and so on [1-7]. MoM has been widely used to numerically simulate scattering from composite model of the object and the underlying rough surface. Yet, after discretized with basis function and tested, the conventional MoM results in a dense impedance matrix. Consequently, the storage, impedance matrix fill-in, and matrix-vector multiplication operations are of $O(N^2)$ complexity, where N is the number of unknowns. To overcome these disadvantages, a number of techniques have been successfully developed to dramatically reduced memory and computational cost with the iterative solution of surface integral equations (SIEs), such as Multilevel fast multipole method (MLFMM) [8-11,13], the adaptive integral method (AIM) [12]. The mathematical basis of MLFMM algorithm is addition theorem. By the addition theorem, the dyadic Green function can be represented in a

Submitted On: Nov. 1, 2011
Accepted On: Oct. 8, 2012

formula in which the observation point and source point are separate. Based on the formula, MLFMM has succeeded in reducing the numerical complexity of memory to $O(N)$ and CPU time to $O(N\log N)$. AIM is FFT-based and for volume integral equations (VIE), it achieve the complexity of $O(N\log N)$.

In this paper, we present an accurate method of moments (MoM) solution of the PMCHWT and EFIE surface integral equations for scattering by 3-D, arbitrarily shaped, homogeneous objects above a 2-D rough surface using hybrid 3DMLUV-ACA method. The object is assumed to be a perfect electric conductor while the rough surface is characterized with Gaussian statistics for surface height and for surface autocorrelation function.

The 3DMLUV method is developed by Deng using EM-interaction-based sampling algorithm. It is an efficient technique to analyze large scale scattering problems and show a computation complexity of $O(N\log N)$. The details of the 3DMLUV can be found in[5,19]. However, before the EM-interaction-based sampling algorithm is used, the original far-field interaction submatrix must be given. When the object or rough surface becomes dielectric, the fast setup method proposed in Reference [19] fails due to the oscillatory nature of the gradient of Green's function. The ACA method [14-16] is purely algebraic; hence, its implementation is integral equation kernel (the gradient of Green's function) independent. Therefore, the ACA method is a perfect choice to speed up the filling of the impedance entries required in 3DMLUV.

The remainder of the paper is organized as follows. In section Ⅱ, we present the implementation of the PMCHWT and EFIE integral equations. The Galerkin method is utilized, where RWG functions are used as both basis and testing functions. The 3DMLUV-ACA is briefly presented. In section Ⅲ, the numerical results are shown, the accuracy of the proposed method is validated first. Finally, bistatic radar cross-section (RCS) of the object/rough surface and difference radar cross-section (d-RCS) [21] of the object are calculated. The influence of the rough surface root mean square (RMS) height, the medium permittivity and the altitude of the object on the scattering characteristic are investigated.

The time factor $\exp(j\omega t)$ is used in this paper and will be suppressed below.

II. THEORY

A. MoM formulation of PMCHWT and EFIE integral equation

As shown in Fig. 1, a 3-D object (PEC) is located above a 2-D random rough surface (Dielectric) and the tapered wave ($\boldsymbol{E}_i$, $\boldsymbol{H}_i$) is employed to avoid rough surface edge scattering effects [22].

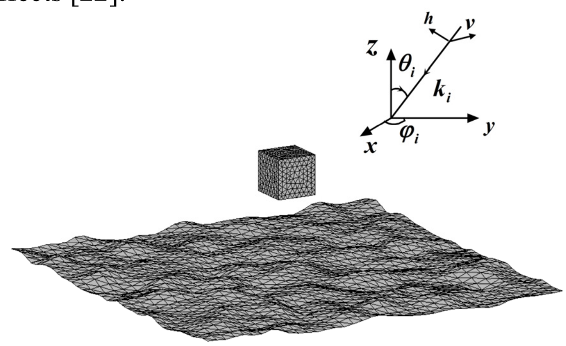

Fig. 1. Composite scattering model of target and rough surface.

The air space, the space object occupied and the space under rough surface are denoted by Region0, Region1 and Region2 while the surface of the object and the rough surface are indicated as S_1 and S_2. The three regions have permittivity and permeability given by ε_0 and μ_0, ε_1 and μ_1, ε_2 and μ_2, respectively. The electric and magnetic fields in Region 0, Region1 and Region2 are $\boldsymbol{E}_0, \boldsymbol{H}_0, \boldsymbol{E}_1, \boldsymbol{H}_1$ and $\boldsymbol{E}_2, \boldsymbol{H}_2$. Since the object is assumed to be PEC, $\boldsymbol{E}_1, \boldsymbol{H}_1$ are all equal to zero.

Using the surface equivalence theorem, the equivalent electric and magnetic current on rough surface and the surface of objects are $\boldsymbol{J}_s, \boldsymbol{M}_s, \boldsymbol{J}_o$ respectively. So the electric and magnetic fields at an arbitrary point $\boldsymbol{r}$ in Region 0 are

$$\begin{aligned}\boldsymbol{E}_0(\boldsymbol{r}) &= \mathrm{Z}_0\boldsymbol{L}_0(\boldsymbol{J}_s) - \boldsymbol{K}_0(\boldsymbol{M}_s)\\ &+ \mathrm{Z}_0\boldsymbol{L}_0(\boldsymbol{J}_o) + \boldsymbol{E}_i(\boldsymbol{r})\end{aligned}, \tag{1a}$$

$$\begin{aligned}\boldsymbol{H}_0(\boldsymbol{r}) &= \frac{1}{\mathrm{Z}_0}\boldsymbol{L}_0(\boldsymbol{M}_s) + \boldsymbol{K}_0(\boldsymbol{J}_s)\\ &+ \boldsymbol{K}_0(\boldsymbol{J}_o) + \boldsymbol{H}_i(\boldsymbol{r})\end{aligned}. \tag{1b}$$

Similarly, the electric and magnetic fields in Region 2 are

$$\boldsymbol{E}_2(\boldsymbol{r}) = \mathrm{Z}_2 \boldsymbol{L}_2(-\boldsymbol{J}_s) - \boldsymbol{K}_2(-\boldsymbol{M}_s), \tag{1c}$$

$$\boldsymbol{H}_2(\boldsymbol{r}) = \frac{1}{\mathrm{Z}_2} \boldsymbol{L}_2(-\boldsymbol{M}_s) + \boldsymbol{K}_2(-\boldsymbol{J}_s), \tag{1d}$$

where operators $\boldsymbol{L}$ and $\boldsymbol{K}$ are given by

$$\boldsymbol{L}_{0,2}(\boldsymbol{X}) = -jk\int [\boldsymbol{X} + \frac{1}{k^2}\nabla(\nabla\cdot\boldsymbol{X})]\mathrm{G}_{0,2} dS', \tag{2a}$$

$$\boldsymbol{K}_{0,2}(\boldsymbol{X}) = -\int \boldsymbol{X} \times \nabla \mathrm{G}_{0,2} dS' . \tag{2b}$$

The vector $\boldsymbol{X}$ represents the surface electric current $\boldsymbol{J}$ and/or the surface magnetic current $\boldsymbol{M}$ on surface S_1 or on surface S_2 . $\mathrm{G}_i = \exp(-jk_i |\boldsymbol{r}-\boldsymbol{r}'|)/4\pi|\boldsymbol{r}-\boldsymbol{r}'|$ is the Green function in homogeneous isotropic medium. $k_i = \omega\sqrt{\varepsilon_i \mu_i}$ is the wave number in Region i . Thus, by equating the tangential component of the electric field $\boldsymbol{E}_0$ to zero, on surface S_1 , we get

$$\begin{aligned}&[\mathrm{Z}_0 \boldsymbol{L}_0(\boldsymbol{J}_s) - \boldsymbol{K}_0(\boldsymbol{M}_s) + \mathrm{Z}_0 \boldsymbol{L}_0(\boldsymbol{J}_o)]|_{\tan} \\ &= -\boldsymbol{E}_i(\boldsymbol{r})|_{\tan}\end{aligned} . \tag{3a}$$

Then, upon equating the tangential component of the electric fields ($\boldsymbol{E}_0$ and $\boldsymbol{E}_2$) and magnetic fields ($\boldsymbol{H}_0$ and $\boldsymbol{H}_2$), on surface S_2 , we get

$$\begin{aligned}&[\mathrm{Z}_0 \boldsymbol{L}_0(\boldsymbol{J}_s) - \boldsymbol{K}_0(\boldsymbol{M}_s) + \mathrm{Z}_0 \boldsymbol{L}_0(\boldsymbol{J}_o) \\ &+ \mathrm{Z}_2 \boldsymbol{L}_2(\boldsymbol{J}_s) - \boldsymbol{K}_2(\boldsymbol{M}_s)]|_{\tan} = -\boldsymbol{E}_i(\boldsymbol{r})|_{\tan}\end{aligned}, \tag{3b}$$

$$\begin{aligned}&[\frac{1}{\mathrm{Z}_0} \boldsymbol{L}_0(\boldsymbol{M}_s) + \boldsymbol{K}_0(\boldsymbol{J}_s) + \boldsymbol{K}_0(\boldsymbol{J}_o) \\ &+ \frac{1}{\mathrm{Z}_2} \boldsymbol{L}_2(\boldsymbol{M}_s) + \boldsymbol{K}_2(\boldsymbol{J}_s)]|_{\tan} = -\boldsymbol{H}_i(\boldsymbol{r})|_{\tan}\end{aligned} . \tag{3c}$$

The equivalent electric and magnetic current $\boldsymbol{J}_s, \boldsymbol{M}_s, \boldsymbol{J}_o$ are approximated by using the RWG vector basis function $\boldsymbol{f}(\boldsymbol{r})$ [23] as follows:

$$\boldsymbol{J}_s(\boldsymbol{r}) = \sum_{n=1}^{P_1} \mathrm{I}_{1n} \boldsymbol{f}_{1n}(\boldsymbol{r}), \tag{4a}$$

$$\boldsymbol{M}_s(\boldsymbol{r}) = \sum_{n=1}^{P_1} \mathrm{I}_{2n} \boldsymbol{f}_{1n}(\boldsymbol{r}), \tag{4b}$$

$$\boldsymbol{J}_o(\boldsymbol{r}) = \sum_{m=1}^{P_2} \mathrm{I}_{3m} \boldsymbol{f}_{2m}(\boldsymbol{r}), \tag{4c}$$

the P_1 and P_2 are the number of unknown coefficients. Upon applying Galerkin's method, the original integral equations are thus transformed into a set of linear equations given by:

$$\begin{bmatrix} \overline{\overline{\boldsymbol{Z}}}_{ss}^{EJ} & \overline{\overline{\boldsymbol{Z}}}_{ss}^{EM} & \overline{\overline{\boldsymbol{Z}}}_{os}^{EJ} \\ \overline{\overline{\boldsymbol{Z}}}_{ss}^{HJ} & \overline{\overline{\boldsymbol{Z}}}_{ss}^{HM} & \overline{\overline{\boldsymbol{Z}}}_{os}^{HJ} \\ \overline{\overline{\boldsymbol{Z}}}_{so}^{EJ} & \overline{\overline{\boldsymbol{Z}}}_{so}^{EM} & \overline{\overline{\boldsymbol{Z}}}_{oo}^{EJ} \end{bmatrix} \begin{bmatrix} \overline{\boldsymbol{I}}_1 \\ \overline{\boldsymbol{I}}_2 \\ \overline{\boldsymbol{I}}_3 \end{bmatrix} = \begin{bmatrix} \overline{\boldsymbol{V}}_s^E \\ \overline{\boldsymbol{V}}_s^H \\ \overline{\boldsymbol{V}}_o^E \end{bmatrix} . \tag{5}$$

where $\overline{\overline{\boldsymbol{Z}}}_{ss}^{EJ}$, $\overline{\overline{\boldsymbol{Z}}}_{ss}^{EM}$, $\overline{\overline{\boldsymbol{Z}}}_{ss}^{HJ}$, $\overline{\overline{\boldsymbol{Z}}}_{ss}^{HM}$ and $\overline{\overline{\boldsymbol{Z}}}_{oo}^{EJ}$ are the impedance submatrices of the rough surface and the object, respectively. The total impedance matrix is complicated by the interactions between the object and rough surface represented by $\overline{\overline{\boldsymbol{Z}}}_{os}^{EJ}$, $\overline{\overline{\boldsymbol{Z}}}_{os}^{HM}$ and $\overline{\overline{\boldsymbol{Z}}}_{so}^{EJ}$, $\overline{\overline{\boldsymbol{Z}}}_{so}^{EM}$. It should be pointed out that, not all of the nine submatrices will be calculated. By using the symmetrical relationship, only six of them will be calculated explicitly, which are $\overline{\overline{\boldsymbol{Z}}}_{ss}^{EJ}$, $\overline{\overline{\boldsymbol{Z}}}_{ss}^{EM}$, $\overline{\overline{\boldsymbol{Z}}}_{ss}^{HM}$, $\overline{\overline{\boldsymbol{Z}}}_{oo}^{EJ}$, $\overline{\overline{\boldsymbol{Z}}}_{so}^{EJ}$, $\overline{\overline{\boldsymbol{Z}}}_{so}^{EM}$. The Bicgstable [20] iterative method will be used to solve equation (5).

B. Tapered incident wave

The tapered incident wave is given by

$$\begin{aligned}\boldsymbol{E}_i &= \exp[-jk(z\cos\theta_i + x\sin\theta_i\cos\phi_i \\ &+ y\sin\theta_i\sin\phi_i)(1+\omega)]\cdot\exp[-t_x - t_y]\end{aligned}, \tag{6}$$

where

$$t_x = \frac{(x\cos\theta_i\cos\phi_i + y\cos\theta_i\sin\phi_i + z\sin\theta_i)^2}{g^2\cos^2\theta_i}, \tag{7a}$$

$$t_y = \frac{(-x\sin\phi_i + y\cos\phi_i)^2}{g^2}, \tag{7b}$$

$$\omega = \frac{1}{k^2}\left(\frac{2t_x - 1}{g^2\cos^2\theta_i} + \frac{2t_y - 1}{g^2}\right), \tag{7c}$$

the θ_i, φ_i are incident angles and g is the tapering parameter. In order to avoid the rough surface edge scattering effects, g must be chosen deliberately with respect to the rough surface length. In this paper, g is taken as $g = L/4$.

C. The Calculation of the RCS and DRCS

Considering the approximation of the Green's function and the gradient of Green's function in the far field regions as:

$$G(\boldsymbol{r},\boldsymbol{r}') \approx \frac{\exp(-jkr)}{4r}\exp(jk(\boldsymbol{k}_s \cdot \boldsymbol{r}')), \quad (8)$$

$$\nabla G(\boldsymbol{r},\boldsymbol{r}') \approx -jkG(\boldsymbol{r},\boldsymbol{r}')\boldsymbol{k}_s. \quad (9)$$

Where

$$\boldsymbol{k}_S = \boldsymbol{x}\sin\theta_s\cos\varphi_s + \boldsymbol{y}\sin\theta_s\sin\varphi_s + \boldsymbol{z}\cos\theta_s,$$

$\boldsymbol{r}$ and $\boldsymbol{r}'$ are the field and source point. θ_s and φ_s are the scattering angles.

The scattered electric field $\boldsymbol{E}_s$ can be calculated by (1a) (after minusing the incident electric field), where the far field approximat-ion (8) and (9) will be used. Defining the difference induced electric and magnetic current as $\boldsymbol{J}_{sd}$ and $\boldsymbol{M}_{sd}$ on the rough surface, the difference electric field can be calculated by:

$$\boldsymbol{E}_{sd}(\boldsymbol{r}) = Z_0\boldsymbol{L}_0(\boldsymbol{J}_{sd}) - \boldsymbol{K}_0(\boldsymbol{M}_{sd}) + Z_0\boldsymbol{L}_0(\boldsymbol{J}_o), \quad (10)$$

Then, the RCS σ and d-RCS σ_d can be given by:

$$\sigma = \lim_{r\to\infty} 4\pi r^2 \frac{|\boldsymbol{E}_s|^2}{|\boldsymbol{E}_i|^2}, \quad (11a)$$

$$\sigma_d = \lim_{r\to\infty} 4\pi r^2 \frac{|\boldsymbol{E}_{sd}|^2}{|\boldsymbol{E}_i|^2}. \quad (11b)$$

D. Fast fill-in method using ACA

When the bottom rough surface is dielectric, for surface integral equations (SIEs), there are two kinds of operators, i.e. the L operator and K operator. The 3DMLUV method fill in the submatrix elements of $\overline{\overline{Z}}^{sub}_{m\times n}$ with the fast method in [19]. Whereas in [19], the target are all assumed to be PEC. So they do not take the K operator into consideration. After discretized by RWG basis function and tested using Galerkin method, the K operator in submatrix $\overline{\overline{\boldsymbol{Z}}}^{EM}_{ss}$ is as follow:

$$\begin{aligned}[\overline{\overline{\boldsymbol{Z}}}^{EM}_{ss}]_{m,n} = &-(\frac{l_m}{2}\boldsymbol{\rho}_m^+(\boldsymbol{r}_m^{c+})\cdot\boldsymbol{H}_{mn}(\boldsymbol{r}_m^{c+}) \\ &+\frac{l_m}{2}\boldsymbol{\rho}_m^-(r_m^{c-})\cdot\boldsymbol{H}_{mn}(\boldsymbol{r}_m^{c-}))\end{aligned}, \quad (13)$$

$$\boldsymbol{H}_{mn}(\boldsymbol{r}_m^{c\pm}) = \int \boldsymbol{f}_n(r')\times\nabla G(\boldsymbol{r}_m^{c\pm},\boldsymbol{r}')ds', \quad (14)$$

where all the symbols have the same meaning as in [23]. Then the normalized area coordinate [23] is introduced to calculate $\boldsymbol{H}_{mn}(\boldsymbol{r}_m^{c\pm})$.

$$\begin{aligned}\boldsymbol{H}_{mn}(\boldsymbol{r}_m^{c\pm}) &= \int \boldsymbol{f}_n(\boldsymbol{r}')\times\nabla G(\boldsymbol{r}_m^{c\pm},\boldsymbol{r}')ds' \\ &= l_n\int(\xi'\boldsymbol{r}_{n1}^+ + \eta'\boldsymbol{r}_{n2}^+ + \zeta'\boldsymbol{r}_{n3}^+ - \boldsymbol{r}_n^+)\times\nabla G(\boldsymbol{r}_m^{c+},\boldsymbol{r}')d\xi'd\eta' \\ &- l_n\int(\xi'\boldsymbol{r}_{n1}^- + \eta'\boldsymbol{r}_{n2}^- + \zeta'\boldsymbol{r}_{n3}^- - \boldsymbol{r}_n^-)\times\nabla G(\boldsymbol{r}_m^{c+},\boldsymbol{r}')d\xi'd\eta'\end{aligned} \quad .(15)$$

therefore, the integrals in (14) can be obtained by calculating the following four integrals:

$$I^{m\pm n\pm} = \int_0^1\int_0^{1-\eta'} \nabla G(r_m^{c\pm},r')d\xi'd\eta', \quad (16)$$

$$I_\xi^{m\pm n\pm} = \int_0^1\int_0^{1-\eta'} \xi'\nabla G(r_m^{c\pm},r')d\xi'd\eta', \quad (17)$$

$$I_\eta^{m\pm n\pm} = \int_0^1\int_0^{1-\eta'} \eta'\nabla G(r_m^{c\pm},r')d\xi'd\eta', \quad (18)$$

$$I_\zeta^{m\pm n\pm} = \int_0^1\int_0^{1-\eta'} \zeta'\nabla G(r_m^{c\pm},r')d\xi'd\eta'. \quad (19)$$

To the far interaction, the approximate relation is given by

$$I_\xi^{m\pm n\pm} = I_\eta^{m\pm n\pm} = I_\zeta^{m\pm n\pm} = \frac{1}{3}I^{m\pm n\pm}. \quad (20)$$

Then, equation (13) can be written as:

$$\begin{aligned}[\overline{\overline{\boldsymbol{Z}}}^{EM}_{ss}]_{m,n} = &-\{\frac{l_m}{2}\boldsymbol{\rho}_m^+(\boldsymbol{r}_m^{c+})\cdot \\ &[(\frac{1}{3}l_n\boldsymbol{r}_{n1}^+ + \frac{1}{3}l_n\boldsymbol{r}_{n2}^+ + \frac{1}{3}l_n\boldsymbol{r}_{n3}^+ - l_n\boldsymbol{r}_n^+)I^{m+n+} \\ &-(\frac{1}{3}l_n\boldsymbol{r}_{n1}^- + \frac{1}{3}l_n\boldsymbol{r}_{n2}^- + \frac{1}{3}l_n\boldsymbol{r}_{n3}^- - l_n\boldsymbol{r}_n^-)I^{m+n-}] \\ &+\frac{l_m}{2}\boldsymbol{\rho}_m^-(r_m^{c-})\cdot[(\frac{1}{3}l_n\boldsymbol{r}_{n1}^+ + \frac{1}{3}l_n\boldsymbol{r}_{n2}^+ + \frac{1}{3}l_n\boldsymbol{r}_{n3}^+ - l_n\boldsymbol{r}_n^+)I^{m-n+} \\ &-(\frac{1}{3}l_n\boldsymbol{r}_{n1}^- + \frac{1}{3}l_n\boldsymbol{r}_{n2}^- + \frac{1}{3}l_n\boldsymbol{r}_{n3}^- - l_n\boldsymbol{r}_n^-)I^{m-n-}]\}\end{aligned} \quad (21)$$

Due to the oscillatory nature of the gradient of Green's function in (16-19), the fast fill-in method proposed in reference [19] breaks down. Therefore, The X, Y, and Z component of (16) will be calculated by ACA method. Because the oscillatory kernel has little impact on ACA. The ACA method has been described in detail in [14-16] and need not be repeated here.

E. The architecture of 3DMLUV-ACA

To present a whole picture of the implementation of 3DMLUV-ACA, we employ a presentation from coarser to finer considerations. Figure 2 shows the architecture of 3DMLUV, where FFI stands for far-field interaction, NFI stands for near-field interaction, MVM stands for matrix-vector multiplication and SVD stands for singular value decomposition. The criterion used to define the FFI and NFI is discussed in detail in [8].

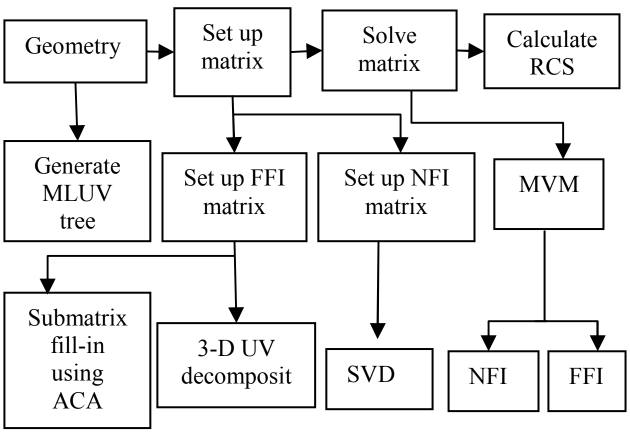

Fig. 2. The architecture of the 3DMLUV-ACA.

Before the UV decomposition is implemented, the FFI submatrix $\overline{\overline{Z}}^{sub}_{m\times n}$ must be calculated, the ACA method is used to speed up the filling as discussed above. Then, the FFI submatrix $\overline{\overline{Z}}^{sub}_{m\times n}$ with low rank r could be approximated by product of a U and V matrix

$$\overline{\overline{Z}}^{sub}_{m\times n} = \overline{\overline{U}}_{m\times r}\overline{\overline{V}}_{r\times n}\ , \qquad (12)$$

where $r << \min(m,n)$. Only $\overline{\overline{U}}_{m\times r}$ and $\overline{\overline{V}}_{r\times n}$ will be stored in memory. Thus, the requirement of storage memory descends from $m\times n$ to $r\times(m+n)$. Moreover, during matrix-vector multiplication in iterative method, the original $\overline{\overline{Z}}^{sub}_{m\times n}\overline{I}^{sub}_{n\times 1}$ will be substituted by $\overline{\overline{U}}_{m\times r}\overline{\overline{V}}_{r\times n}\overline{I}^{sub}_{n\times 1}$, which greatly reduce the computational complexity.

III. RESULS AND DEICUSSIONS

A. Accuracy and efficiency

The CPU employed below is Intel Core I7 2.8GHz processor with 2G Bytes of RAM.

To validate the 3DMLUV solution of PMCHWT integral equations, for plane wave with $\theta_i = 0^\circ, \varphi_i = 90^\circ$, the VV-polarized bistatic RCS of a dielectric sphere with radius of $r = 3\lambda$ (λ is the wavelength in free space) in free space is calculated and compared with Mie series in Fig. 3. The relative permittivity $\varepsilon_r = 4$ and the number of unknowns is 86,400. For efficiency analysis, the MLFMM is also used to calculate the scattering of the same sphere The memory requirement and computational time consumed are compared in Table 1.

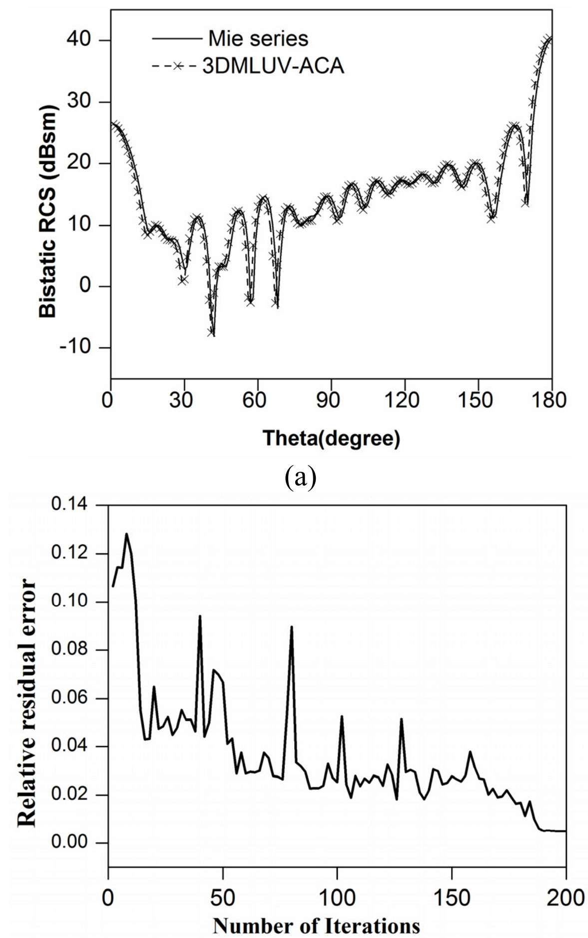

Fig. 3. (a) Bistatic RCS of a dielectric sphere; (b) Number of iterations.

Table 1: Memory Requirements and Relative Computational Time.

Method	Unknowns	Memory(MB)	Time(s)
MLFMM	86,400	978	2027
3DMLUV	86,400	946	2160

From Fig. 3 and Table 1, it can be concluded that 3DMLUV-ACA not only show a high computation accuracy but also is highly efficient. The memory 3DMLUV method needed is even lower than the MLFMM method. But because of the fill-in time consumed by 3DMLUV, the computation time needed is slightly more than MLFMM method.

B. Statistic composite EM scattering

In this section, statistic composite scattering is presented and discussed by making 100 Monte Carlo simulations of the rough surface. The tapered incident wave with $\theta_i = 30^\circ, \varphi_i = 90^\circ$ is used for all experiments below.

Case 1: Given surface length $L_x = L_y = 16\lambda$, correlation length $l_x = l_y = 0.5\lambda$, RMS height $h = 0.04\lambda$, the relative dielectric permittivity $\varepsilon_r = 2.5 - 0.18j$. let a PEC cube with side length of $a = 2\lambda$ lie at altitudes of $d = 2\lambda, 10\lambda$ respectively. Figure 4 presents the VV-polarized DRCS. Because the object at the lower altitude has more intense interaction with the underlying rough surface, the DRCS for $d = 2\lambda$ is generally larger than that for $d = 10\lambda$.

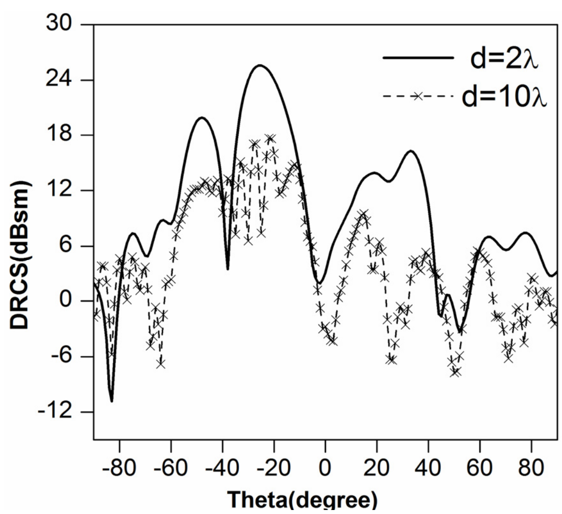

Fig. 4. DRCS of the cube above rough surface for different altitude.

Case 2: Considering a cylinder with a radius of $R = 1\lambda$ and a length of $H = 3\lambda$ lie at an altitude of $d = 3\lambda$ above the dielectric Gaussian rough surface. The rough surface has the same parameters as in Case 1 except that the RMS heights vary as $h = 0.01\lambda, 0.02\lambda, 0.08\lambda$. Figure 5 gives the VV-polarize RCS. It is obviously that the composite bistatic RCS is closely correlated with RMS heights. The composite RCS appears as a peak near $\theta_s = -30^\circ$, which is more significant for the smoother surface with lower value of h. And the incoherent scattering increases while the coherent scattering decreases as the roughness increases.

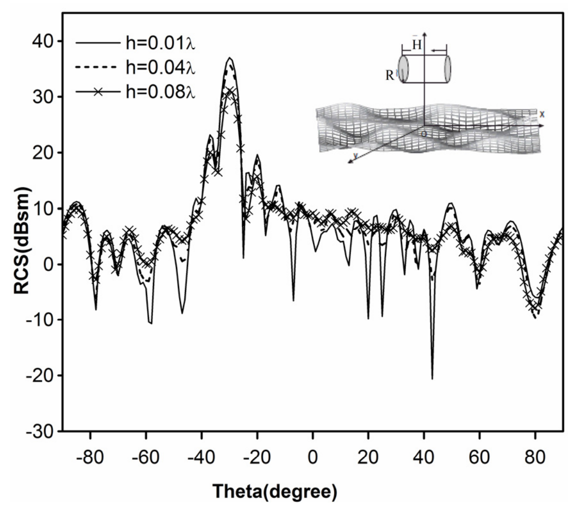

Fig. 5. RCS of the cylinder above rough surface for different RMS heights.

Case 3: let a PEC sphere with radius of $r = 1.5\lambda$ lie at an altitude of $d = 3\lambda$ above a Gaussian dielectric rough surface. The rough surface has the same parameters as in Case 1. Figure 6 presents the composite HH-polarized bistatic RCS and DRCS for different permittivities. The imaginary part of the permittivity is kept the same while the real part of the permittivity vary as 2.5, 5 and 10.

From Fig. 6, we can see that the permittivity also has an important influence on the scattering characteristic. The surface with higher permittivity has higher reflectance. So the composite RCS and DRCS is larger for rough surface with higher permittivity.

IV. CONCLUSION

The 3DMLUV/ACA method is proposed to simulate the scattering from the dielectric objects. By investigating the bistatic electromagnetic scattering from the composite model of a 3-D arbitrarily shaped object located above a 2-D Gaussian dielectric rough surface, this method is proved to be accurate and highly efficient. Furthermore, due to the algebraic nature of 3DMLUV/ACA, this method can be easily extended to the composite scattering of dielectric object located above the dielectric rough surface with a few modifications.

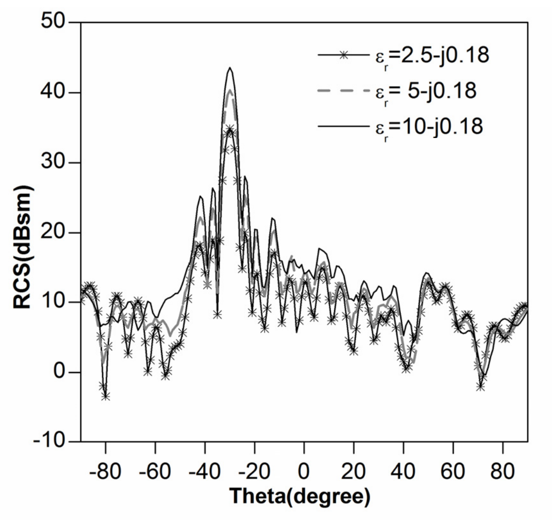

(a)

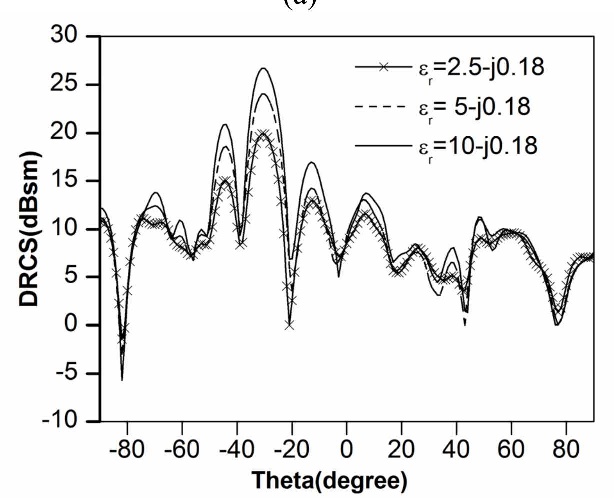

(b)

Fig. 6. RCS and DRCS of the sphere above rough surface for different permittivities.

ACKNOWLEDGMENT

This work was supported by the National Science Foundation of China (Grant No. 61001059, Grant No.41140034), the China Postdoctoral Science Foundation, and the Fundamental Research Funds for the Central Universities.

REFERENCES

[1] E. A. Shtager, "An Estimation of Sea Surface Influence on Radar Reflectivity of Ships," *IEEE Trans. Antennas Propagat.,* vol. 47, no. 10, pp. 1623-1627, Oct. 1999.

[2] R. J. Burkholder, M. R. Pino, and F. Obelleiro, "A Monte Carlo Study of the Rough Sea Surface Influence on the Radar Scattering from 2-D Ships," *IEEE Trans. on Antennas Propagat. Mag.*, vol. 43, no. 2, 25-33, Apr. 2001.

[3] M. R. Pino, R. J. Burkholder and F. Obelleiro, "Spectral Acceleration of the Generalized Forward-Backward Method," *IEEE Trans. Antennas Propagat.*, vol. 50, no. 6, pp.785-797, Jun. 2002.

[4] K. Jamil., R. J. Burkholder, "Radar Scattering from a Rolling Target Floating on a Time-evolving Rough Sea Surface," *IEEE Trans. Geosci. Remote Sens.*, vol. 44, no. 11, pp. 3330-3337, 2006.

[5] F.S. Deng, S.Y. He, H.T. Chen, W.D. Hu, W.X. Yu, and G.-Q. Zhu, Numerical Simulat-ion of Vector Wave Scattering from the Target and Rough Surface Composite Model with 3-D Multilevel UV Method, *IEEE Trans. Antennas Propagat.*, vol. 58 , pp. 1625-1634, 2010

[6] S. Y. He, C. Li, F. Zhang, G. Q. Zhu, W. D. Hu, W. X. Yu, "An Improved MM-PO Method with UV Technique for Scattering from an Electrically Large Ship on a Rough Sea Surface at Low Grazing Angle," *Applied Computational Electromagnetics Society (ACES) Journal*, vol. 26, no. 2, pp. 87-95, February 2011.

[7] J. Li, L. X. Guo, H. Zeng, "FDTD Investigation on Electromagnetic Scattering from Two-Dimensional Layered Rough Surfaces," *Applied Computational Electrom-agnetics Society (ACES) Journal*, vol. 25, no. 5, pp. 450 - 475, May 2010.

[8] C. C. Lu and W. C. Chew, "A Multilevel Algorithm for Solving a Boundary Integral Equation of Wave Scattering," *Microw. Opt. Tech. Lett.*, vol. 7, no. 10, pp. 456-461, Jul. 1994.

[9] J. M. Song and W. C. Chew, "Multilevel Fast Multipole Algorithm for Solving Combined Field Integral Equation of Electromagnetic Scattering," *Microw. Opt. Tech. Lett.*, vol. 10, no. 1, pp. 14-19, Sep. 1995.

[10] H. Zhao, J. Hu, and Z. Nie, "Parallelization of MLFMA with Composite Load Partition Criteria and Asynchronous Communication," *Applied Computational Electromagnetic Society (ACES) Journal*, vol. 25, no. 2, pp. 167-173, 2010.

[11] H. Fangjing, Z. Nie, and J. Hu, "An Efficient Parallel Multilevel Fast Multipole Algorithm for Large-Scale Scattering Problems," *Applied Computational Electromagnetic Society (ACES) Journal*, vol. 25, no. 4, pp. 381-387, 2010.
[12] E. Bleszynski, M. Bleszynski, and T. Jaroszewicz, "AIM: Adaptive Integral Method for Solving Large-scale Electromagnetic Scattering and Radiation Problems," *Radio Sci.*, vol. 31, no. 5, pp. 1225-1251, May 1996.
[13] M. Li, H. Chen, C. Li, R. Chen, C. Ong, "Hybrid UV/MLFMA Analysis of Scattering by PEC Targets above a Lossy Half-Space," *Applied Computational Electromagnetics Society (ACES) Journal*, vol. 26, no. 1, pp. 17 - 25, January 2011.
[14] K. Z. Zhao, M. N. Vouvakis, and J. F. Lee, "The Adaptive Cross Approximation Algorithm for Accelerated Method of Moments Computations of EMC Problems," *IEEE Trans. Electromagn. Compat.*, vol. 47, no. 4, pp. 763-773, Nov. 2005.
[15] Z. Liu, R. Chen, J. Chen, Z. Fan, "Using Adaptive Cross Approximation for Efficient Calculation of Monostatic Scattering with Multiple Incident Angles," *Applied Computational Electromagnetics Society (ACES) Journal*, vol. 26, no. 4, pp. 325-333, April 2011.
[16] R. S. Chen, Z. H. Fan, Y. Y. An, M. M. Zhu, K. W. Leung, "Modified Adaptive Cross Approximation Algorithm for Analysis of Electromagnetic Problems," *Applied Computational Electromagnetics Society (ACES) Journal*, vol. 26, no. 2, pp. 160-169, February 2011.
[17] L. Tsang, D. Chen, P. Xu, Q. Li, and V. Jandhyala, "Wave Scattering with the UV Multilevel Partitioning Method: 1. Two-dimensional Problem of Perfect Electric Conductor Surface Scattering," *Radio Sci.*, vol. 39, no. 5, pp. RS5010, 2004.
[18] L.Tsang, Q. Li, P. Xu et al, "Wave Scattering with the UV Multilevel Partitioning Method: 2. Three-dimensional Problem of Nonpenetrable Surface Scattering," *Radio Sci.*, vol. 39, no. 5, RS5011, 2004.
[19] H. T. Chen, J. X. Luo and G. Q. Zhu, "Using UV Technique to Accelerate the MM-PO Method for Three-dimensional Radiation and Scattering Problem," *Microwave Opt. Technol. Lett.*, vol. 48, no. 8, pp.1615 -1618, 2006.
[20] E. Topsakal, R. Kindt, K. Sertel and J. Volakis, "Evaluation of the BiCGSTAB(l) Algorithm for Finite-element/Boundary-integral Method," *IEEE Trans. Antennas Propagat. Mag.*, vol. 43, no. 6, pp.124- 131, Dec.2001.
[21] H. X. Ye, Y. Q. Jin, "Fast Iterative Approach to Difference Scattering from the Object Above a Rough Surface," *IEEE Trans. Geosci. Remote Sens.*, vol. 44, no. 1, pp. 108-115, Jan. 2006.
[22] H. X. Ye, Y. Q. Jin, "Parameterization of the Tapered Incident Wave for Numerical Simulation of Electromagnetic Scattering from Rough Surface," *IEEE Trans. Antennas Propagat.,* vol. 53 no. 3, pp. 1234-1237, Mar. 2005.
[23] S. M. Rao, D. R.Wilton, and A.W. Glisson, "Electromagnetic Scattering by Surfaces of Arbitrary Shape," *IEEE Trans. Antennas Propagat.*, vol. AP-30, pp. 409-418, May 1982.

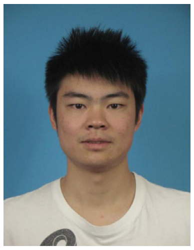

C. Li was born in 1986. He received the B.S degree in information countermeasure technology from North University of China, Taiyuan, in 2008. He is currently working towards the Ph.D degree in Radio Physics at Wuhan University, Wuhan, China. His current research interests are electromagnetic inverse scattering, computational electromagnetic method, microwave imaging and time domain echo analysis.

S. Y. He was born in 1982. She received the telecommunication engineering degree and the Ph.D. degree in Radio Physics from Wuhan University, Wuhan, China, in 2003 and 2009, respectively. She is currently a associate professor in Wuhan Universtiy. From 2005 to 2006, she was a Research Assistant in Wireless Communications Research Centre, City University of Hong Kong. Her research interests include EM theory and its application, computational electromagnetic, and radar imaging.